Halide-Directed Synthesis of Square Prismatic Ag Nanocrystals by

the Polyol Method

Su-Wen Hsu¹ and Andrea R. Tao^{1,2*}

¹NanoEngineering Department, University of California, San Diego

9500 Gilman Drive MC 0448, La Jolla, CA 92093-0448

²Materials Science and Engineering, University of California, San Diego

9500 Gilman Drive MC 0448, La Jolla, CA 92093-0448

*E-mail: atao@eng.ucsd.edu

Abstract

Achieving shape control of high-quality metal nanocrystals is a critical challenge in the

fabrication of bottom-up plasmonic materials. Here, we synthesize a uniquely anisotropic Ag

nanocrystal shape using a modified polyol method. Single-crystalline Ag square prism

nanocrystals— which possess two square facets and four rectangular facets— with uniform size

distributions and high yield (up to 96%) are generated by the controlled addition of Br⁻ anions

during the nucleation and growth process. Br acts as a reshaping agent for the generation of

single-crystalline seed nanoparticles that direct subsequent anisotropic growth in the <100>

direction. Nanocrystal growth and shape development is monitored through optical absorption

spectroscopy, which reveals the localized surface plasmon resonances of the square prisms. Electrodynamic simulations indicate strong near-field enhancement associated with the high aspect-ratio shape, and indicates the potential application of these nanocrystals as optical nanoantenna in plasmonic platforms, such as surface-enhanced Raman spectroscopy sensors and optoelectronic junctions.

Introduction

Shaped metal nanocrystals, especially those composed of Au and Ag, possess unique optical properties that result from the excitation of localized surface plasmon resonances (LSPRs), where collective oscillations of conduction electrons are excited by incident light. Anisotropic shapes are known to provide a strong enhancement of the electric field localized near sharp nanocrystal corners or edges, and have been demonstrated for applications in surface-enhanced Raman scattering (SERS), 1-3 optical labeling and imaging, 4 chemical sensing, 5 and diagnostics. 6 For example, Ag nanocubes (AgNCs) have been employed in a number of device architectures including plasmonic nanocomposites embedded in polymer membrane, 7 deposited onto solid supports as surface-enhanced Raman scattering (SERS) chips, 8 modified with lipid bilayers as protein-binding sensors, 9, 10 and assembled as metal-insulator-metal junctions for light generation. 11

Colloidal synthesis has been demonstrated to produce a wide variety of Ag nanocrystal shapes such as cubes, octahedrons, bars, bipyramids, plates, decahedrons, rods, and wires with high yields (> 80 %) and in a scalable manner. 12-25 In many cases, shape control is achieved by the addition of a chemical stabilizing agent that coordinates to specific crystal facets during nanocrystal growth. This selectivity is typically attributed to: (i) lattice matching of a given crystal plane with the molecular geometry of the coordinating agent, 26 or (ii) site-selective binding where strong coordination only occurs at specific atomic or surface features. 14, 27 One common and important synthetic method for producing shaped metal nanocrystals is the polyol method, where metal salt precursors and a chemical stabilizing agent are reacted in a polyol solvent (e.g. ethylene glycol 14, 21 or pentanediol 13). Polyols serve as a mild reducing agent and are particularly well-suited for nanoparticle synthesis given their relatively high boiling points,

temperature-dependent reducing power, and the ability to solubilize a variety of metal precursors. Poly(vinyl pyrrolidone) (PVP) has been demonstrated as a useful surface protecting agent in the polyol reaction because it can coordinate readily to metal ions through the pyrolidone functional group and is also highly soluble in polyol solvents. For example, PVP has been shown to direct the polyol synthesis of AgNCs and symmetry-related shapes such as cuboctahedra and octahedra. These resulting shapes have been attributed to the ability of PVP to coordinate selectively to Ag{100} facets over other low-energy crystal planes.

More recently, a number of anisotropic shapes beyond AgNCs have been demonstrated using various modifications of the general PVP-assisted polyol method described earlier. 12, 13, 21, 22 Methods for tailoring shape include microwave-assisted reduction, where microwaves provide homogeneous and fast heating (compared with conventional heating methods utilized in colloidal synthesis) of the reaction bath to promote uniform seed nucleation – the nucleation sites for nanocrystal growth – and controlled nanocrystal growth rate. 28, 29 The use of ionic additives to the polyol reaction has also been successful for nanocrystal shape optimization.^{21, 22, 30} For example, Wiley et al. demonstrated that Ag nanobars and triangular bipyramids could both be obtained using the PVP-assisted polyol method upon the addition of Br to an AgNC reaction mixture. Zheng et al. confirmed that Br participates in a selective etching mechanism, where spherical seed particles are generated at the expense of cube-shaped particles.³¹ The addition of Br results in the oxidation of Ag⁰ to AgBr, which is a soluble product under polyol reaction conditions. The authors observed that differently shaped seeds could be obtained at varying Br concentrations. For low [Br] where the ratio of [Ag⁺]/[Br-] precursors is high, multiply-twinned seeds were etched away to leave only singly-twinned seeds that produced elongated bipyramid nanocrystals. For higher [Br-] where the ratio of [Ag+]/[Br-] precursors is low, only singlecrystalline seeds are generated. These seeds grow into nanobars resembling an elongated cube structure, possessing two square facets and four rectangular facets (Figure 1).^{21, 22} Chloride-assisted polyol methods have also been reported to generate the controlled growth of various nanocrystals shapes such as octahedra, nanocubes, nanowires, and multipods, as well as shaped composite nanocrystals composed of Ag, Au, Rh, and Pd.^{18, 30, 32-37} However, the reason for this preferred anisotropy (over the more symmetric nanocube shape) is unclear.

Here, we explore the shape control offered by Br⁻ addition to the PVP-assisted polyol method to produce a unique shape with anisotropy related to AgNCs and nanobars: Ag square prisms (AgSPs). Just as rods and disks represent two extreme forms of ellipsoids, AgSPs and nanobars represent two extreme forms of AgNCs. Diametric to nanobars, AgSPs are elongated nanocubes but they possess large aspect-ratios where height (H) is smaller than length (L). We demonstrate that AgSPs can be generated by tailoring the [Ag⁺]/[Br⁻] ratio in the polyol reaction, producing a single-crystalline structure capped by Ag{100} facets. The LSPRs of the resulting nanocrystals can be tuned through synthetic control of H and L.

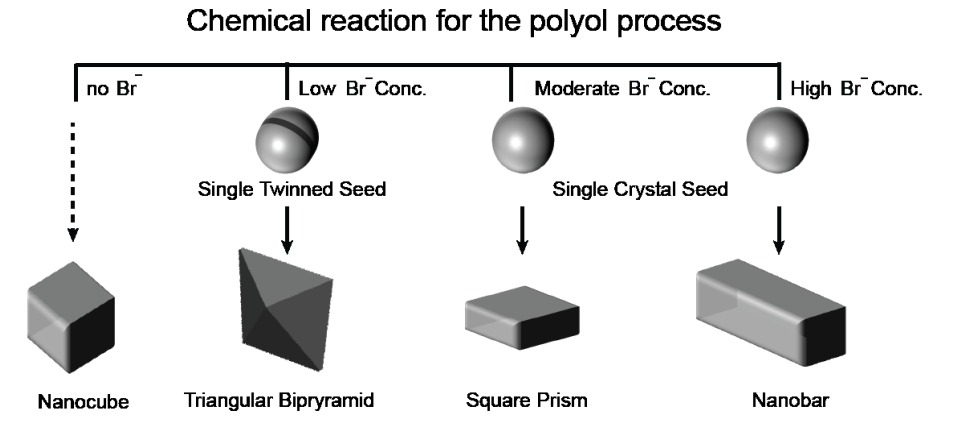


Figure 1. Schematic shows the effect of bromide ion concentration on the crystal structure of seed and shape of nanocrystal in bromide additive polyol synthesis.

Results and Discussion

We have developed a modified polyol process to fabricate AgSP nanocrystals with tunable sizes ranging from 20.3 to 46.1 nm in height and from 56.9 nm to 82.4 nm in length. In this synthesis, ethylene glycol (EG) acts as the solvent; EG and its derivatives, such as glycolaldehyde generated from oxidation of ethylene glycol, serve as reducing agents; and PVP serves as a capping ligand for anisotropic nanocrystal formation. (Figure 2). The reaction mixture is made by adding 10 mL EG and 50μ L of 1mM NaBr solution in EG to a flask and heated in an oil bath at 145°C for 1h. To this reaction mixture, a 6 mL AgNO₃ solution in EG (16.67mg/mL) and a 6mL PVP and NaBr solution in EG (16.67mg of PVP/ mL and 0.0125mg of NaBr/mL) were added dropwise via syringe pump at a rate of 1 mL/min. We monitored this reaction by UV-visible absorption spectroscopy.

Our results confirm that Br⁻ addition results in the formation of AgSPs (Figure 2a) with uniform shape and size distribution. This result from two contributing factors: (1) moderate Br⁻ concentration and (2) a lower growth temperature. The growth of AgSP nanocrystals begins with the formation of near-spherical single-crystal seeds, followed by anisotropic growth into AgSPs (Supporting information, S2 and S3). Compared to Ag nanobars where growth is inhibited in two of the three orthogonal <100> directions, the shape of the square prism results from inhibited growth in only one <100> direction. This arises from the lower Br⁻ content, which discourages the AgBr etching reaction from occurring over the entire the nanocrystal surface (Supporting information, S7). We also observe a slower nanocrystal growth rate when using a lower reaction temperature than employed in the AgNC synthesis, which may contribute to more uniform

colloidal dispersions (Supporting information, S7). Figure 2b shows the extinction spectra of reaction mixture for various reaction times (t_{rxn}) in the range of 10-360 min. The extinction spectrum shows the formation of pseudo-spherical nanocrystals at the beginning of the reaction, indicated by a single absorption maximum at 405 nm. Electron microscopy confirms that these seeds possess average diameters of 10.3 ± 0.73 nm (Supporting information, S2). Anisotropic growth and the formation of AgSPs is indicated by the growth of four separate extinction peaks in the visible region over the reaction period. (See Supporting Information, S1). At t_{rxn} =60 min, we observe three extinction peaks at 515 nm (dipole LSPR), 410 nm, and 360 nm (higher order mode of LSPR), indicating the formation of an anisotropic nanocrystal shape. Scanning electron microscope (SEM) images of the AgSP nanocrystals ("top-view") show that the dispersion consists of nanocrystals with uniform square facets (Figure 2c) and images taken at a 45° tilt ("tilt-view") shows that L>H (Figure 2d). With increased reaction time, the dipolar LSPR peak at 515 nm red-shifts while an extinction peak at 475 nm (quadrupolar mode of LSPR) appears at t_{rxn} = 150 min and intensifies over time (Figure 2b).

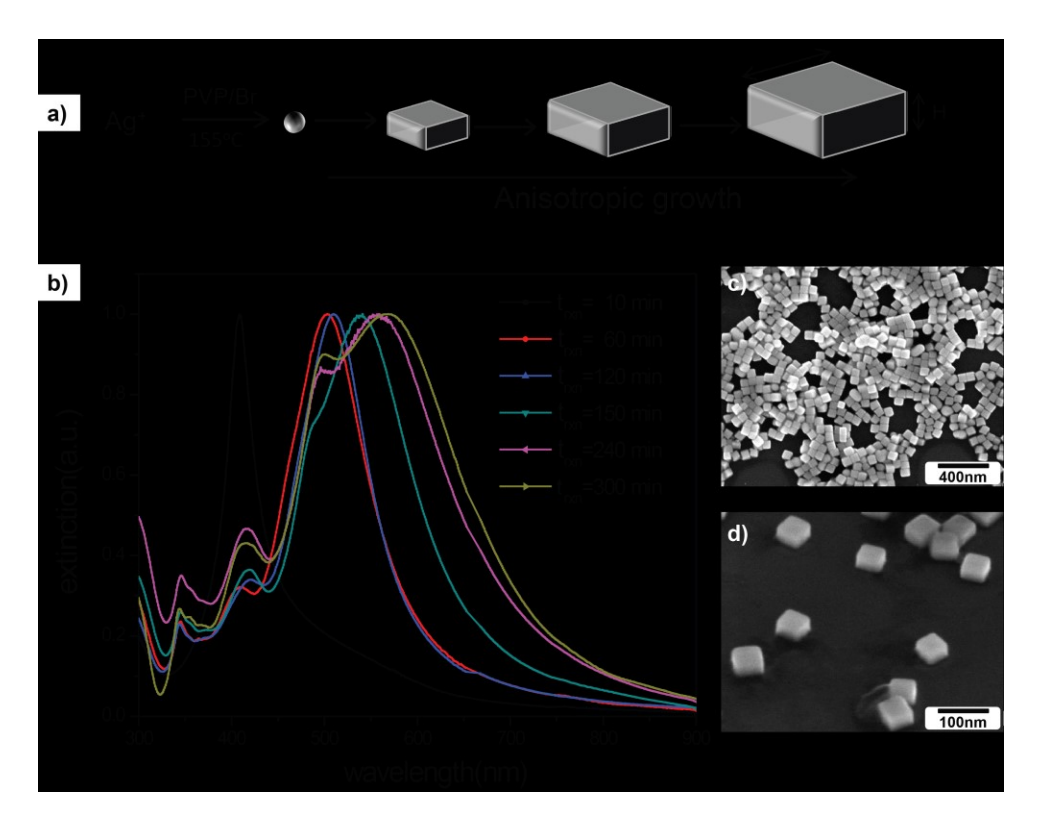


Fig 2. a) Schematic shows that square prism NPs formation under the polyol synthetic method. The morphology of Ag NPs changes from small spherical-like to bigger square prism with increasing the reaction time. Here, the bromide ion acts an important role for anisotropic growth of square prism. b) The extinction spectra of spherical-like and three different square prisms colloidal solution with different reaction time, t_{rxn} . c) Top view of square prism shows the length of square facet is uniform. d) SEM image with 45° titling shows length, L > height, H.

In order to characterize the size distribution of the resulting AgSP dispersion, we measured the average length (L_{av}) of AgSPs by top-view SEM imaging of >200 nanocrystals and the average height (H_{av}) of AgSPs tilt-view SEM imaging (at 90°) of >100 nanocrystals. The size of AgSPs $(L_{av} \text{ and } H_{av})$ is observed to increase exponentially with extending t_{rxn} . At t_{rxn} = 1h, the L_{ave} and H_{av} of the AgSPs are 56.9 ± 2.94 nm and 20.3 ± 0.90 nm, respectively. After elongating t_{rxn} to 8h, L_{av} increases to 82.4 \pm 4.02 nm and H_{av} increases to 46.1 \pm 2.44 nm, as shown in the histogram in Figure 3(a-d). The insets in Figure 3 show SEM images for a single AgSP rotated at 45° to clearly confirm that L>H for each t_{rxn} .

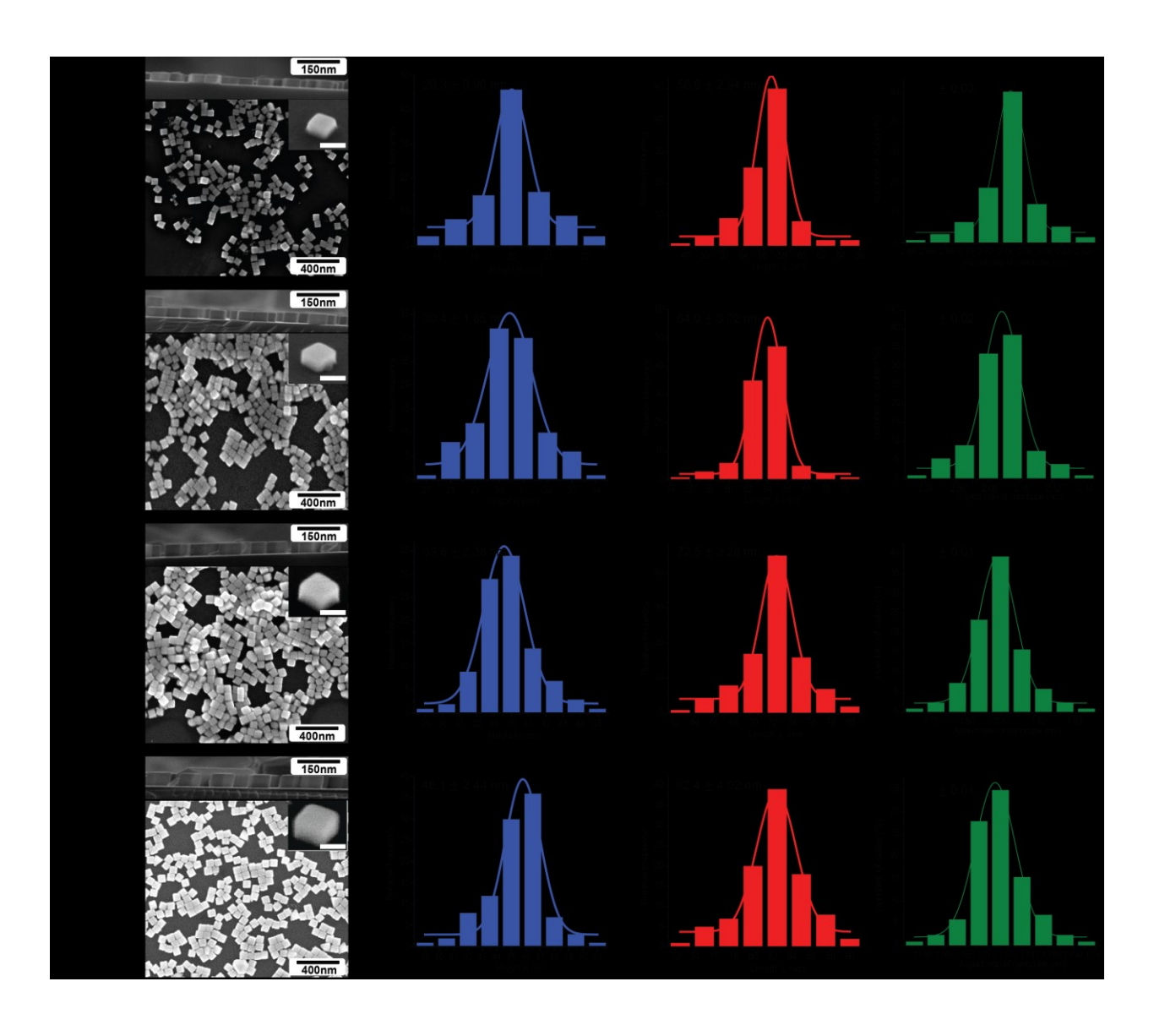


Fig 3. The shape and size distribution of square prisms with 1hr, 2hr, 4hr, and 5hr at 155°C in (a-d), respectively. The size distributions of the square prisms were characterized by SEM imaging to measure the average of length, L_{ave} , and cross-sectional (tilted by 90°) imaging to measure the average of height, H_{ave} and aspect ratio (AR) of square prism. L_{ave} is calculated from more than 200 square prisms. The histograms show that L_{ave} = 56.9 \pm 2.94 nm, 64.0 \pm 3.02 nm, 72.5 \pm 3.28 nm, and 82.4 \pm 4.02 nm for the corresponding prism samples in (a-d), respectively. H_{ave} and AR of square prism are measured over more than 100 square prisms from cross-section SEM images. The histograms show that H_{ave} =20.3 \pm 0.90 nm, 30.4 \pm 1.85 nm, 39.6 \pm 2.38 nm, and 46.1 \pm 2.44 nm for the corresponding samples in (a-d), respectively. The histograms show that AR of square prism = 2.74 \pm 0.03 nm, 2.08 \pm 0.02, 1.81 \pm 0.01 nm, and 1.77 \pm 0.01 for the corresponding samples in (a-d), respectively. The inset shows SEM images for single square prism rotated by 45°, clearly showing that L > H. Scale bar: 65 nm

In order to confirm the crystal morphologies of the AgSPs, we compared the XRD spectrum for two different sample preparations: (i) a powder sample of dried AgSPs (randomly oriented nanocrystals), and (ii) close-packed AgSP films deposited on a Si substrate (aligned nanocrystals). This close-packed film is fabricated by Langmuir–Blodgett deposition, where the square facets of the AgSPs are oriented parallel to the air-water interface (and thus, parallel to the Si substrate) due to the hydrophilic nature of the PVP-coated AgSP surfaces (inset in Figure 4b). The XRD spectrum of the powder sample is shown in Figure 4a, and indicates that AgSPs are crystalline, but that X-ray scattering from the (100) family of crystal planes is dominant due to nanocrystal shape. The XRD spectrum of the aligned sample shows the (200) peak is even more greatly enhanced, indicating that the square facets are (100) terminated.

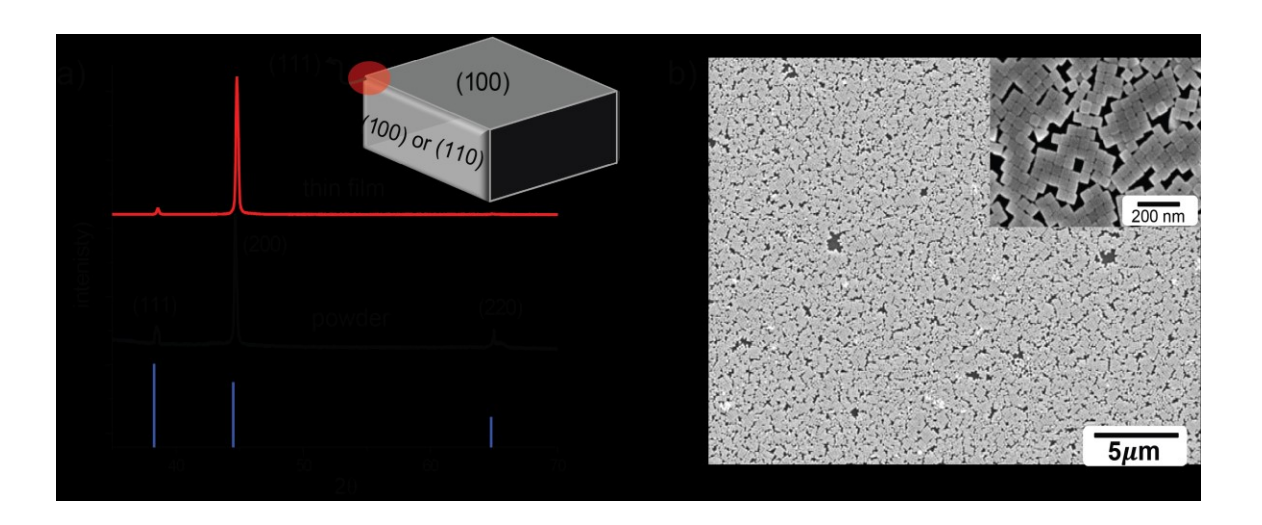


Fig 4. Characterization of crystal structure and orientation square prisms. a) The XRD spectra of: a powder sample of dried square prisms (black line), a close-packed nanoprism film deposited on a Si substrate (red line), and the ideal face-centered cubic (fcc) Ag (JCPDS File 04-0783, blue vertical line). The (200) peak is strongly enhanced in the close-packed film, indicating that the square facets of prisms belong to the (100) family of crystal planes. b) SEM image of a close-packed square prism film fabricated by Langmuir-Blodgett deposition. The inset image shows that the square facet of the prism is oriented parallel to the substrate.

The LSPRs of the AgSPs can be assigned by carrying out finite-difference time-domain (FDTD) calculations using the Lumerical software package. We calculated the extinction cross-section of an AgSP with L=85 nm and H=45 nm (blue line, Figure 5b) which we expect to be consistent with the extinction spectrum of the colloidal solution with $L_{av} = 82.4 \pm 4.02$ nm and $H_{av} = 46.1$ \pm 2.44 nm (black line in Figure 5b). The extinction cross-section is obtained by adding the crosssections for incident light polarized in three orthogonal directions (as insert schematic in Figure 5a): x-polarization (black dashed), y-polarization (red dashed), and z-polarization (blue dashed). The extinction spectrum shows four peaks, in contrast with three peaks observed for the smaller AgSPs with L_{ave} = 56.9± 2.94 nm and H_{ave} = 20.3 ± 0.90 nm (supporting information S4). The lowest energy peaks for both AgSP sizes (at 600 nm and 515 nm, respectively) results from xand y-polarized excitation. The electric field distributions (Figure 5c and S4) and vector plot (Supporting information S5 and S6) indicate these peaks correspond to the dipole LSPR modes where the field is localized in the eight corners of the AgSP. This dipole mode undergoes an 85 nm red-shift with increasing L_{av} from 56.9 nm to 82.4 nm (See time-dependent of extinction spectrum in S1). Comparing the plasmonic modes of AgNCs with similar edge lengths to those of the AgSPs, the dipole mode of AgNCs only exhibit a ~36 nm red-shift when the edge length is increased from 57 nm to 82.5 nm. 16, 38 Thus, the dipole LSPR of AgSPs is much more sensitive to nanocrystal size, volume effects, and aspect-ratio than the dipole LSPR of AgNCs. This has important consequences in the ability to tune the resonance wavelength associated with intense near-field localization, which is difficult to carry out for highly symmetric shapes such as AgNCs whose LSPRs can only be tuned through size and volume effects. In addition, AgSPs exhibit sharped corners and edges that facilitate more intense near-field localization than other nanocrystal shapes (triangular nanoplates, nanorods, and nanodisks) whose LSPR wavelengths

can be broadly tuned by controlling aspect-ratio, but do not exhibit as strong near-field enhancements.^{39, 40} The second lowest energy peak (475 nm) results from y- and z-polarized excitation (red and blue dashed lines in Figure 5a) and field distributions also show localization in the corners of the AgSP. This LSPR mode only shows up at the size of AgSPs beyond a critical size where L_{av} > 65 nm and H_{av} > 30 nm (Figure 2b). This mode intensifies without a significant shift in wavelength when AgSP size is increased. The remaining two high energy LSPR peaks (410 nm and 360 nm) stem from excitation with all three polarization directions and possess wavelengths that are independent of nanocrystal size. The electron field distribution of these two modes in the xy-plane and xz-plane (Figure 5e,f and S4d,e) indicate that these two peaks correspond to higher order LSPR modes where the field is localized near the AgSP facets and edges.

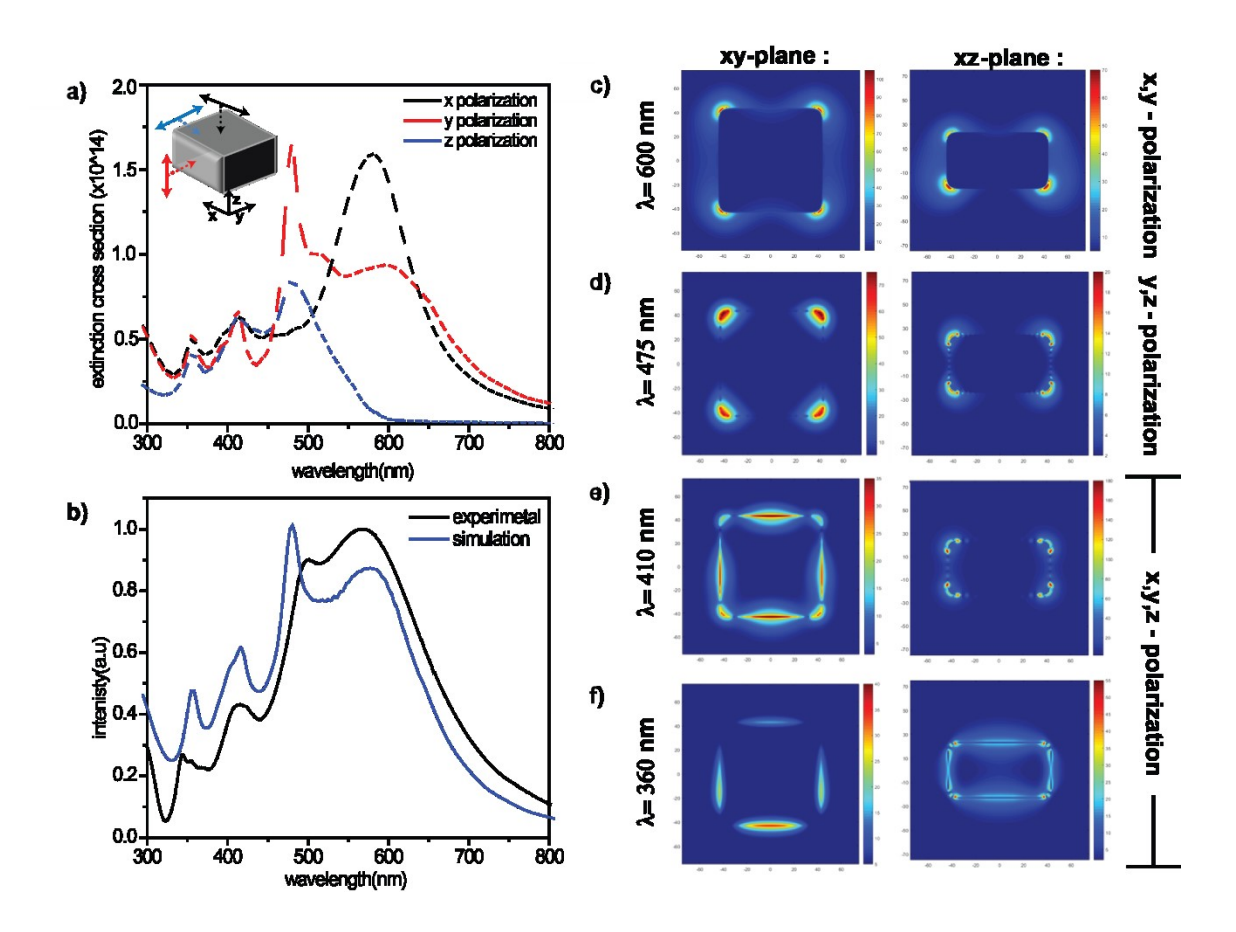


Fig 5. a) FDTD simulations of the extinction cross-section for a square prism with L=85 nm and H=45 nm for x-polarization (black dashed line) and z-polarization (red dashed line). b) The experimental (black) extinction spectrum of colloidal square prism nanoparticles dispersed in ethanol with L=82.4 \pm 4.02 nm and H=46.1 \pm 2.44 nm. For comparison, we plotted the simulated extinction cross-section (blue) resulting from the sum of x-polarization, y-polarization, and z-polarization. c-f) Color maps for the simulated optical near-field at four different wavelengths: at 600, 475, 410 and 360 nm, respectively, which correspond with the four peaks at FDTD calculated and experimental extinction spectra.

Conclusions

We have demonstrated the fabrication of AgSP nanocrystals with uniform size distributions and high-yield by a modified polyol synthesis. This single-crystalline nanostructure is capped by Ag{100} facets and experience anisotropic growth such that H < L. The unique AgSP shape demonstrates that the [Ag+]/[Br-] ratio in the polyol reaction serves as a determinant of nanocrystal growth rate in the <100> direction by controlling the kinetics of Ag⁺ reduction. Like other highly anisotropic plasmonic nanocrystals, AgSPs exhibit LSPRs that are sensitive to its overall shape morphology. The degree of AgSP anisotropy dictates overlap of the dipolar and quadrupolar LSPR modes, with better LSPR mode separation occurring for increased H:L ratios. This work provides a rational pathway for the chemical synthesis of anistropic Ag nanocrystals whose optical response can be tuned through aspect-ratio. We expect this to further the application of colloidal materials in plasmonics and metamaterials that rely on the precise fabrication of shaped optical antenna.

Materials and Methods

Chemicals and Materials

Silver nitrate (AgNO₃ Fisher), Ethylene glycol (EG, J. T, Baker), poly (vinyl pyrrolidone) (PVP, Mw=55,000, Aldrich), sodium bromide (NaBr, J.T. Baker), ethanol (CH₃OH, Goldshield chemical), chloroform (CHCl₃, Aldrich).

Synthesis of Ag square prisms

10mL ethylene glycol (EG) was added to a 50mL and 50µL, 1 mM NaBr (0.103mg NaBr in 1mL EG) in glass flask which was placed in an oil bath setting at 145°C for 1h with magnetic stirring. Two solutions were simultaneously injected into glass flask with an injection rate of 1mL per minutes by syringe pump. One solution contained 100 mg AgNO3 in 6mL EG, the other contained 100 mg PVP and 0.075 mg NaBr in 6mL EG. The color of solution changes from yellow, yellow-orange, orange, orangish pink, yellowish pink, to pink opaque. The nanocrystal undergoes the anisotropic growth into square prism-shaped nanoparticle. The size of square prisms can be controlled by reaction time. The size of square prisms can be controlled by reaction time. The reaction time can be extended from 1-6 hours where longer reaction times result in increasing both height and length of the AgSPs, but a reduced overall aspect-ratio. The colloidal solution was washed with ethanol and DI water (volume ratio of ethanol: DI water=1:1) twice to remove the un-reaction precursor (Ag⁺) and excess PVP. During the washing process, the 22ml colloidal solution with 22ml ethanol/water mixture was centrifuged at 3,400 rpm for 15min. Finally, Ag square prism-shaped nanoparticles was dispersed in EG for storage and further characterization.

Fabrication of Ag square prisms orderly array for XRD and cross sectional SEM

Silicon substrates were sonicated in ethanol for removing dust and then further cleaned in a freshly prepared piranha solution of 70% (v) concentrated H₂SO₄ and 30% (v) H₂O₂ for removing the organic materials. To prepare the orderly composite film, as-made square prims

colloidal 1ml was diluted in a 3ml ethanol and then precipitated for removing free PVP twice. The square prism was dispersed in 1 ml CHCl₃. A glass petri dish was thoroughly rinsed with ethanol and DI water. The colloidal nanocrystal solution was then added dropwise to the air—water interface of the petri dish, leaving an isotropically distributed monolayer of NCs floating at the air—water interface. After the desired amount of colloidal solution was added, the film was allowed to equilibrate for about 15 min. Nanocrystal monolayers were then transferred onto the clean Silicon substrate by dip-coating. The orderly array of square prism on silicon substrate was cut and mounted vertically for measurement the height of square prism by cross sectional SEM. For the thin film XRD sample, the isotropically distribution monolayer of NCs in air-water interface was further compressed to form the close packed thin film with square plane of square prism parallel to air-water interface and then transfer to silicon substrate by dip-coating.

Associated content

Supporting Information

The Supporting Information is available free of charge on the ACS Publications website at DOI: XXXXXXXXX.

Figures S1–S7: time-dependent of extinction spectrum; size distribution of spherical-like seed; time-dependent SEM image of the shape of nanocrystals; FDTD simulation extinction cross-section of square prism nanocrystals; electron field distribution and vector plot of square prism nanocrystals; effect of shape of nanocrystals on Br- concentration and reaction temperature/time.

Author information

Corresponding Authors

*E-mail: atao@eng.ucsd.edu

ORCID

Su-Wen Hsu: 0000-0001-6553-3201

Andrea R. Tao: 0000-0003-1857-8743

Conflicts of interest

The authors declare no competing financial interest.

Acknowledgments

This work is financially supported by the Defense Advanced Research Projects Agency (DARPA) Microsystems Technology Office (W911NF-16-2-0156). We acknowledge UCSD's Nano3 facility for use of their scanning electron microscopes.

References

- Mulvihill, M. J.; Ling, X. Y.; Henzie, J.; Yang, P. D., Anisotropic Etching of Silver Nanoparticles for Plasmonic Structures Capable of Single-Particle SERS. J. Am. Chem. Soc. 2010, 132, 268-274.
- 2. Yoon, I.; Kang, T.; Choi, W.; Kim, J.; Yoo, Y.; Joo, S. W.; Park, Q. H.; Ihee, H.; Kim, B., Single Nanowire on a Film as an Efficient SERS-Active Platform. *J. Am. Chem. Soc.* **2009**, *131*, 758-762.
- 3. Mulvihill, M.; Tao, A.; Benjauthrit, K.; Arnold, J.; Yang, P., Surface-enhanced Raman spectroscopy for trace arsenic detection in contaminated water. *Angew. Chem. Int. Ed.* **2008**, *47*, 6456-6460.
- 4. Lee, K. S.; El-Sayed, M. A., Gold and silver nanoparticles in sensing and imaging: Sensitivity of plasmon response to size, shape, and metal composition. *J. Phys. Chem. B* **2006**, *110*, 19220-19225.
- 5. Anker, J. N.; Hall, W. P.; Lyandres, O.; Shah, N. C.; Zhao, J.; Van Duyne, R. P., Biosensing with plasmonic nanosensors. *Nat. Mater.* **2008,** *7*, 442-453.
- 6. Rosi, N. L.; Mirkin, C. A., Nanostructures in biodiagnostics. Chem. Rev. 2005, 105, 1547-1562.
- Ke, Y.; Meng, G. W.; Huang, Z. L.; Zhou, N. N., Electrosprayed large-area membranes of Ag-nanocubes embedded in cellulose acetate microspheres as homogeneous SERS substrates. *J. Mater. Chem. C* 2017, 5, 1402-1408.
- 8. Dill, T. J.; Rozin, M. J.; Brown, E. R.; Palani, S.; Tao, A. R., Investigating the effect of Ag nanocube polydispersity on gap-mode SERS enhancement factors. *Analyst* **2016**, *141*, 3916-3924.
- 9. Galush, W. J.; Shelby, S. A.; Mulvihill, M. J.; Tao, A.; Yang, P. D.; Groves, J. T., A Nanocube Plasmonic Sensor for Molecular Binding on Membrane Surfaces. *Nano Lett.* **2009**, *9*, 2077-2082.
- Wu, H. J.; Henzie, J.; Lin, W. C.; Rhodes, C.; Li, Z.; Sartorel, E.; Thorner, J.; Yang, P. D.; Groves, J. T., Membrane-protein binding measured with solution-phase plasmonic nanocube sensors. *Nat. Methods* 2012, 9, 1189-U1181.
- 11. Qian, H. H., S.-W.; Gurunatha, K.; Zhao, J.; Riley, C.T.; Lu, D.; Tao, A.R.; and Liu, Z., Investigation of the light generation from crystalline Ag-cubes based metal-insulator-metal tunnel junctions. CLEO: OELS Fundamental Science 2017, San Jose, California United States 14–19 May 2017, OSA
- 12. Zeng, J.; Zheng, Y. Q.; Rycenga, M.; Tao, J.; Li, Z. Y.; Zhang, Q. A.; Zhu, Y. M.; Xia, Y. N., Controlling the Shapes of Silver Nanocrystals with Different Capping Agents. *J. Am. Chem. Soc.* **2010**, *132*, 8552-8553.

- 13. Tao, A.; Sinsermsuksakul, P.; Yang, P. D., Polyhedral silver nanocrystals with distinct scattering signatures. *Angew. Chem. Int. Ed.* **2006**, *45*, 4597-4601.
- 14. Sun, Y. G.; Xia, Y. N., Shape-controlled synthesis of gold and silver nanoparticles. *Science* **2002**, *298*, 2176-2179.
- 15. Kundu, S.; Maheshwari, V.; Niu, S.; Saraf, R. F., Polyelectrolyte mediated scalable synthesis of highly stable silver nanocubes in less than a minute using microwave irradiation. *Nanotechnology* **2008**, *19*, *065604*.
- 16. Zhang, Q. A.; Li, W. Y.; Wen, L. P.; Chen, J. Y.; Xia, Y. N., Facile Synthesis of Ag Nanocubes of 30 to 70 nm in Edge Length with CF3COOAg as a Precursor. *Chem. Eur. J.* **2010**, *16*, 10234-10239.
- 17. Yu, D. B.; Yam, V. W. W., Controlled synthesis of monodisperse silver nanocubes in water. *J. Am. Chem. Soc.* **2004**, *126*, 13200-13201.
- 18. Wiley, B.; Herricks, T.; Sun, Y. G.; Xia, Y. N., Polyol synthesis of silver nanoparticles: Use of chloride and oxygen to promote the formation of single-crystal, truncated cubes and tetrahedrons. *Nano Lett.* **2004**, *4*, 1733-1739.
- Fan, F. R.; Liu, D. Y.; Wu, Y. F.; Duan, S.; Xie, Z. X.; Jiang, Z. Y.; Tian, Z. Q., Epitaxial growth of heterogeneous metal nanocrystals: From gold nano-octahedra to palladium and silver nanocubes. *J. Am. Chem.* Soc. 2008, 130, 6949-6951.
- 20. Wiley, B.; Sun, Y. G.; Xia, Y. N., Synthesis of silver nanostructures with controlled shapes and properties. *Acc. Chem. Res.* **2007**, *40*, 1067-1076.
- 21. Wiley, B. J.; Chen, Y. C.; McLellan, J. M.; Xiong, Y. J.; Li, Z. Y.; Ginger, D.; Xia, Y. N., Synthesis and optical properties of silver nanobars and nanorice. *Nano Lett.* **2007**, *7*, 1032-1036.
- 22. Wiley, B. J.; Xiong, Y. J.; Li, Z. Y.; Yin, Y. D.; Xia, Y. N., Right bipyramids of silver: A new shape derived from single twinned seeds. *Nano Lett.* **2006**, *6*, 765-768.
- Sanchez-Iglesias, A.; Winckelmans, N.; Altantzis, T.; Bals, S.; Grzelczak, M.; Liz-Marzan, L. M., High-Yield Seeded Growth of Monodisperse Pentatwinned Gold Nanoparticles through Thermally Induced Seed Twinning.
 J. Am. Chem. Soc. 2017, 139, 107-110.
- 24. Xiong, Y. J.; Cai, H. G.; Wiley, B. J.; Wang, J. G.; Kim, M. J.; Xia, Y. N., Synthesis and mechanistic study of palladium nanobars and nanorods. *J. Am. Chem. Soc.* **2007**, *129*, 3665-3675.

- 25. Hong, B. H.; Bae, S. C.; Lee, C. W.; Jeong, S.; Kim, K. S., Ultrathin single-crystalline silver nanowire arrays formed in an ambient solution phase. *Science* **2001**, *294*, 348-351.
- Yu, S. H.; Colfen, H.; Mastai, Y., Formation and optical properties of gold nanoparticles synthesized in the presence of double-hydrophilic block copolymers. *J. Nanosci. Nanotechnol.* 2004, 4, 291-298.
- 27. Johnson, C. J.; Dujardin, E.; Davis, S. A.; Murphy, C. J.; Mann, S., Growth and form of gold nanorods prepared by seed-mediated, surfactant-directed synthesis. *J. Mater. Chem.* **2002**, *12*, 1765-1770.
- 28. Tsuji, M.; Hashimoto, M.; Nishizawa, Y.; Kubokawa, M.; Tsuji, T., Microwave-assisted synthesis of metallic nanostructures in solution. *Chem. Eur. J.*, **2005**, *11*, 440-452.
- 29. Tsuji, M.; Hashimoto, M.; Nishizawa, Y.; Tsuji, T., Preparation of gold nanoplates by a microwave-polyol method. *Chem. Lett.* **2003**, *32*, 1114-1115.
- 30. Im, S. H.; Lee, Y. T.; Wiley, B.; Xia, Y. N., Large-scale synthesis of silver nanocubes: The role of HCl in promoting cube perfection and monodispersity. *Angew. Chem. Int. Ed.* **2005**, *44*, 2154-2157.
- 31. Zhang, Q.; Moran, C. H.; Xia, X. H.; Rycenga, M.; Li, N. X.; Xia, Y. N., Synthesis of Ag Nanobars in the Presence of Single-Crystal Seeds and a Bromide Compound, and Their Surface-Enhanced Raman Scattering (SERS) Properties. *Langmuir* **2012**, *28*, 9047-9054.
- 32. Li, Z. Q.; Tao, J.; Lu, X. M.; Zhu, Y. M.; Xia, Y. N., Facile synthesis of ultrathin Au nanorods by aging the AuCl(oleylamine) complex with amorphous Fe nanoparticles in chloroform. *Nano Lett.* **2008**, *8*, 3052-3055.
- 33. Korte, K. E.; Skrabalak, S. E.; Xia, Y. N., Rapid synthesis of silver nanowires through a CuCl- or CuCl2-mediated polyol process. *J. Mater. Chem.* **2008**, *18*, 437-441.
- 34. Biacchi, A. J.; Schaak, R. E., The Solvent Matters: Kinetic versus Thermodynamic Shape Control in the Polyol Synthesis of Rhodium Nanoparticles. *Acs Nano* **2011**, *5*, 8089-8099.
- 35. Zettsu, N.; McLellan, J. M.; Wiley, B.; Yin, Y. D.; Li, Z. Y.; Xia, Y. N., Synthesis, stability, and surface plasmonic properties of rhodium multipods, and their use as substrates for surface-enhanced Raman scattering. *Angew. Chem. Int. Ed.* **2006**, *45*, 1288-1292.
- 36. Zhang, H.; Jin, M. S.; Xiong, Y. J.; Lim, B.; Xia, Y. N., Shape-Controlled Synthesis of Pd Nanocrystals and Their Catalytic Applications. *Acc. Chem. Res.* **2013**, *46*, 1783-1794.

- 37. Liu, M. C.; Zheng, Y. Q.; Zhang, L.; Guo, L. J.; Xia, Y. N., Transformation of Pd Nanocubes into Octahedra with Controlled Sizes by Maneuvering the Rates of Etching and Regrowth. *J. Am. Chem. Soc.* **2013**, *135*, 11752-11755.
- 38. Zhang, Q. A.; Li, W. Y.; Moran, C.; Zeng, J.; Chen, J. Y.; Wen, L. P.; Xia, Y. N., Seed-Mediated Synthesis of Ag Nanocubes with Controllable Edge Lengths in the Range of 30-200 nm and Comparison of Their Optical Properties. *J. Am. Chem. Soc.* **2010**, *132*, 11372-11378.
- 39. Wiley, B.; Sun, Y. G.; Mayers, B.; Xia, Y. N., Shape-controlled synthesis of metal nanostructures: The case of silver. *Chem. Eur. J.* **2005**, *11*, 454-463.
- 40. Mayer, M.; Scarabelli, L.; March, K.; Altantzis, T.; Tebbe, M.; Kociak, M.; Bals, S.; de Abajo, F. J. G.; Fery, A.; Liz-Marzan, L. M., Controlled Living Nanowire Growth: Precise Control over the Morphology and Optical Properties of AgAuAg Bimetallic Nanowires. *Nano Lett.* 2015, 15, 5427-5437.

Table of Contents (ToC) Graphic

